Beneficial effect of human anti-amyloid-beta active immunization on neurite morphology and tau pathology

Serrano-Pozo, A ; William, C M ; Ferrer, I ; Uro-Coste, E ; Delisle, M B ; Maurage, C A ; Hock, C ; Nitsch, R M ; Masliah, E ; Growdon, J H ; Frosch, M P ; Hyman, B T

Abstract: Anti-amyloid-beta immunization leads to amyloid clearance in patients with Alzheimer's disease, but the effect of vaccination on amyloid-beta-induced neuronal pathology has not been quantitatively examined. The objectives of this study were to address the effects of anti-amyloid-beta active immunization on neurite trajectories and the pathological hallmarks of Alzheimer's disease in the human hippocampus. Hippocampal sections from five patients with Alzheimer's disease enrolled in the AN1792 Phase 2a trial were compared with those from 13 non-immunized Braak-stage and age-matched patients with Alzheimer's disease, and eight age-matched non-demented controls. Analyses included neurite curvature ratio as a quantitative measure of neuritic abnormalities, amyloid and tau loads, and a quantitative characterization of plaque-associated neuritic dystrophy and astrocytosis. Amyloid load and density of dense-core plaques were decreased in the immunized group compared to non-immunized patients ($P < 0.01$ and $P < 0.001$, respectively). The curvature ratio in non-immunized patients with Alzheimer's disease was elevated compared to non-demented controls ($P < 0.0001$). In immunized patients, however, the curvature ratio was normalized when compared to non-immunized patients ($P < 0.0001$), and not different from non-demented controls. In the non-immunized patients, neurites close to dense-core plaques (within 50 microm) were more abnormal than those far from plaques (i.e. beyond 50 microm) ($P < 0.0001$). By contrast, in the immunized group neurites close to and far from the remaining dense-core plaques did not differ, and both were straighter compared to the non-immunized patients ($P < 0.0001$). Compared to non-immunized patients, dense-core plaques remaining after immunization had similar degree of astrocytosis ($P = 0.6060$), more embedded dystrophic neurites ($P < 0.0001$) and were more likely to have mitochondrial accumulation ($P < 0.001$). In addition, there was a significant decrease in the density of paired helical filament-1-positive neurons in the immunized group as compared to the non-immunized ($P < 0.05$), but not in the density of Alz50 or thioflavin-S positive tangles, suggesting a modest effect of anti-amyloid-beta immunization on tangle pathology. Clearance of amyloid plaques upon immunization with AN1792 effectively improves a morphological measure of neurite abnormality in the hippocampus. This improvement is not just attributable to the decrease in plaque load, but also occurs within the halo of the remaining dense-core plaques. However, these remaining plaques still retain some of their toxic potential. Anti-amyloid-beta immunization might also ameliorate the hippocampal tau pathology through a decrease in tau phosphorylation. These data agree with preclinical animal studies and further demonstrate that human anti-amyloid-beta immunization does not merely clear amyloid from the Alzheimer's disease brain, but reduces some of the neuronal alterations that characterize Alzheimer's disease.

DOI: https://doi.org/10.1093/brain/awq056

Journal Article
Published Version

Originally published at:
Serrano-Pozo, A; William, C M; Ferrer, I; Uro-Coste, E; Delisle, M B; Maurage, C A; Hock, C; Nitsch, R M; Masliah, E; Growdon, J H; Frosch, M P; Hyman, B T (2010). Beneficial effect of human anti-amyloid-beta active immunization on neurite morphology and tau pathology. Brain: A Journal of Neurology, 133(5):1312-1327.
DOI: https://doi.org/10.1093/brain/awq056

doi:10.1093/brain/awq056 Brain 2010: 133; 1312–1327 | 1312

BRAIN
A JOURNAL OF NEUROLOGY

Beneficial effect of human anti-amyloid-β active immunization on neurite morphology and tau pathology

Alberto Serrano-Pozo,[1,2] Christopher M. William,[1] Isidro Ferrer,[3] Emmanuelle Uro-Coste,[4] Marie-Bernadette Delisle,[4] Claude-Alain Maurage,[5] Christoph Hock,[6] Roger M. Nitsch,[6] Eliezer Masliah,[7] John H. Growdon,[1] Matthew P. Frosch[1,8] and Bradley T. Hyman[1]

1 MassGeneral Institute for Neurodegenerative Disease, Massachusetts General Hospital, Massachusetts Alzheimer Disease Research Center, Harvard Medical School, Building 114, 16th Street, 02129-4404, Charlestown, MA, USA
2 Servicio de Neurología, Instituto de Biomedicina de Sevilla (IBiS), Hospitales Universitarios Virgen del Rocío, Av. Manuel Siurot s/n 41013 Seville, Spain
3 Institut Neuropatologia-Servei Anatomia Patològica, IDIBELL-Hospital Universitari de Bellvitge, Hospitalet de Llobregat, 08907 Barcelona, Spain
4 Service d'Anatomie Pathologique et Histologie-Cytologie, CHU de Toulouse, Faculté de Médicine Rangueil, INSERM U858, 31432 Toulouse, France
5 Université Lille Nord de France, INSERM U837, F-59000 Lille, France
6 Division of Psychiatry Research, University of Zurich, 8008 Zurich, Switzerland
7 Department of Neuroscience and Department of Pathology, University of California-San Diego School of Medicine, La Jolla, 92093-0624 CA, USA
8 C. S. Kubik Laboratory for Neuropathology, Massachusetts General Hospital, 55 Fruit Street, 02114, Boston, MA, USA

Correspondence to: Bradley T. Hyman, MD, PhD,
Building 114,16th Street-2009,
Charlestown,
MA 02129-4404, USA
E-mail: bhyman@partners.org

Anti-amyloid-β immunization leads to amyloid clearance in patients with Alzheimer's disease, but the effect of vaccination on amyloid-β-induced neuronal pathology has not been quantitatively examined. The objectives of this study were to address the effects of anti-amyloid-β active immunization on neurite trajectories and the pathological hallmarks of Alzheimer's disease in the human hippocampus. Hippocampal sections from five patients with Alzheimer's disease enrolled in the AN1792 Phase 2a trial were compared with those from 13 non-immunized Braak-stage and age-matched patients with Alzheimer's disease, and eight age-matched non-demented controls. Analyses included neurite curvature ratio as a quantitative measure of neuritic abnormalities, amyloid and tau loads, and a quantitative characterization of plaque-associated neuritic dystrophy and astrocytosis. Amyloid load and density of dense-core plaques were decreased in the immunized group compared to non-immunized patients ($P<0.01$ and $P<0.001$, respectively). The curvature ratio in non-immunized patients with Alzheimer's disease was elevated compared to non-demented controls ($P<0.0001$). In immunized patients, however, the curvature ratio was normalized when compared to non-immunized patients ($P<0.0001$), and not different from non-demented controls. In the non-immunized patients, neurites close to dense-core plaques (within 50 μm) were more abnormal than those far from plaques (i.e. beyond 50 μm) ($P<0.0001$). By contrast, in the immunized group neurites close to and far from the remaining dense-core plaques did not differ, and both were straighter compared to the non-immunized patients ($P<0.0001$). Compared to non-immunized patients, dense-core plaques remaining after immunization had similar degree of astrocytosis ($P=0.6060$), more embedded dystrophic neurites ($P<0.0001$) and were more likely to have mitochondrial accumulation ($P<0.001$). In addition, there was a significant decrease in the density of paired helical filament-1-positive neurons in the immunized group as compared to the non-immunized ($P<0.05$), but not in the density of Alz50 or thioflavin-S positive tangles, suggesting a modest effect of

Received November 9, 2009. Revised February 10, 2010. Accepted February 15, 2010. Advance Access publication March 31, 2010

anti-amyloid-β immunization on tangle pathology. Clearance of amyloid plaques upon immunization with AN1792 effectively improves a morphological measure of neurite abnormality in the hippocampus. This improvement is not just attributable to the decrease in plaque load, but also occurs within the halo of the remaining dense-core plaques. However, these remaining plaques still retain some of their toxic potential. Anti-amyloid-β immunization might also ameliorate the hippocampal tau pathology through a decrease in tau phosphorylation. These data agree with preclinical animal studies and further demonstrate that human anti-amyloid-β immunization does not merely clear amyloid from the Alzheimer's disease brain, but reduces some of the neuronal alterations that characterize Alzheimer's disease.

Keywords: Alzheimer's disease; amyloid; immunization; AN1792

Abbreviations: Aβ = amyloid-β; DAPI = 4′,6-diamidino-2-phenylindole; PHF1 = paired helical filament-1; VDAC1 = voltage-dependent anion-selective channel protein 1

Introduction

The major pathological hallmarks of Alzheimer's disease are neuronal loss, amyloid senile plaques and neurofibrillary tangles within the cerebral cortex (Braak and Braak, 1991). Senile plaques are extracellular deposits of amyloid-β (Aβ) peptide, a byproduct of the metabolism of the amyloid precursor protein after its sequential cleavage by the β- and γ-secretases. Neurofibrillary tangles are intraneuronal somatic aggregates comprised of the microtubule-stabilizing protein tau, which is abnormally hyperphosphorylated. Other pathological findings include synaptic loss in cortical areas, as well as astrogliosis and microgliosis surrounding senile plaques; cerebral amyloid angiopathy (i.e. Aβ deposits in the wall of cortical and leptomeningeal vessels) is a common concomitant pathological process. Clinicopathological studies have shown that neurofibrillary tangles, synaptic loss and neuronal loss correlate with dementia progression and severity better than amyloid deposits (DeKosky and Scheff, 1990; Terry *et al.*, 1991; Gómez-Isla *et al.*, 1996, 1997). However, substantial biochemical and genetic evidence points to Aβ as an essential trigger for the disease (Hardy and Selkoe, 2002). Aβ might directly trigger a cascade of pathogenic events that lead to synaptic and dendritic abnormalities, neurofibrillary tangles and neuronal death, but the course down these pathways to disease may remain dependent on Aβ or might become independent of Aβ once initiated. The latter proposal raises the possibility that therapies directed at reduction in brain levels of Aβ might not be capable of preventing the progression of dementia.

Immunotherapy against Aβ, either through active immunization with Aβ aggregates or by passive transfer of anti-Aβ antibodies, has proven to be effective in the prevention of Aβ deposition and the clearance of already existing Aβ plaques in a number of transgenic mouse models of Alzheimer's disease (Schenk *et al.*, 1999; Bard *et al.*, 2000; Bacskai *et al.*, 2001, 2002; DeMattos *et al.*, 2001; Lemere *et al.*, 2003; Wilcock *et al.*, 2004). Moreover, both active and passive immunization approaches prevented, improved or even reversed the memory deficits described in those mouse models (Janus *et al.*, 2000; Morgan *et al.*, 2000; Dodart *et al.*, 2002; Kotilinek *et al.*, 2002). Also, an amelioration of tau pathology has been reported after anti-Aβ immunization in several mouse models with both amyloid plaques and neuronal tau aggregates (Oddo *et al.*, 2004, 2008; Wilcock *et al.*, 2009).

The first immunotherapy clinical trial in patients with Alzheimer's disease was an active immunization trial with a pre-aggregated preparation of synthetic human Aβ42 (AN1792). The phase 2a of this trial was halted due to the occurrence of subacute meningoencephalitis among some patients in the treatment group, so that patients only received one to three injections out of the four doses initially planned (Orgogozo *et al.*, 2003). Despite the interruption of the trial, a modest but significant positive effect of immunization on some cognitive and functional outcome measures has been documented (Hock *et al.*, 2003; Gilman *et al.*, 2005). Recently, two long-term follow-up studies have yielded conflicting results, with no difference in the rates of survival to death and progression to severe dementia in subjects from an earlier phase 1 trial (Holmes *et al.*, 2008) and a reduced rate of functional decline in a subset of subjects from the phase 2a trial (Vellas *et al.*, 2009).

To date, the effects of AN1792 immunization on Alzheimer's disease neuropathology have been reported in five single case reports (Nicoll *et al.*, 2003; Ferrer *et al.*, 2004; Masliah *et al.*, 2005; Bombois *et al.*, 2007; Uro-Coste *et al.*, 2010) and one case series (Boche *et al.*, 2008; Holmes *et al.*, 2008). These neuropathological findings can be summarized as (i) significant reduction in amyloid load, with relative abundance of the collapsed or 'moth-eaten' morphology among the remaining plaques; (ii) increased extension and severity of cerebral amyloid angiopathy and increased frequency of cerebral amyloid angiopathy-related microhaemorrhages; (iii) decreased density of dystrophic neurite clusters; (iv) reduced density of reactive astrocytes clusters; (v) decreased density of activated microglia clusters, with some examples of microglial cells engulfing amyloid-β fibrils; and (vi) advanced neurofibrillary pathology (i.e. Braak stages V–VI). Interestingly, the amount of remaining amyloid load seems to correlate inversely with the anti-Aβ antibody titres in serum (Holmes *et al.*, 2008).

While there is evidence of the beneficial effects of active and passive anti-amyloid immunization on neurite morphology and synapses in Alzheimer's disease mouse models (Lombardo *et al.*, 2003; Buttini *et al.*, 2005; Brendza *et al.*, 2005; Spires-Jones *et al.*, 2009), little is known about the effects of AN1792 on neurites and neurons in the human Alzheimer's disease brain. Although there was a description of the appearance of collapsed 'moth-eaten' plaques, the characteristics of the amyloid plaques remaining after immunization have not been well described.

Additionally, the relationship between Aβ clearance and neurofibrillary tangles, tau phosphorylation and aggregation status has not been fully documented in AN1792-treated patients.

The present study was aimed at (i) addressing the effect of AN1792 on Aβ-related neurite abnormalities; (ii) characterizing the properties of amyloid plaques remaining after immunization; and (iii) characterizing the phosphorylation and aggregation status of neuronal tau after AN1792 immunization.

Materials and methods

Brain specimens

Formalin-fixed paraffin-embedded sections from the hippocampus of five patients who participated in the phase 2a active immunization trial with AN1792 (Elan-Wyeth Pharmaceuticals, Inc.) were compared with the hippocampal sections from non-demented controls ($n = 8$) and patients with Alzheimer's disease ($n = 13$) from the Massachusetts Alzheimer Disease Research Center Brain Bank. All the study subjects or their next-of-kin gave written informed consent for the brain donation at their respective institutions and the Massachusetts General Hospital Institutional Review Board approved the study protocol. Four of the immunized patients with Alzheimer's disease have been previously described as single reports (Ferrer *et al*., 2004; Masliah *et al*., 2005; Bombois *et al*., 2007; Uro-Coste *et al*., 2010). The three groups were matched by age and gender. Immunized patients and non-immunized Alzheimer's disease subjects were also matched by Braak stage (Table 1 and Supplementary Table 1).

Quantitative immunohistochemical studies

Eight-micrometre-thick sections were deparaffinized for immunohistochemistry by standard methods. Primary and secondary antibodies, pretreatments for antigen retrieval and developing strategies are listed in Supplementary Table 3. To minimize variability, all sections were stained in single batches. Negative controls lacking primary antibody were performed in parallel for all experiments. Immunohistochemical staining was performed with 3,3′-diaminobenzidine (Vector Lab, Burlingame, CA), counterstained with haematoxylin, dehydrated with increasing concentrations of ethanol, cleared with xylene and coverslipped with Permount® mounting media (Fisher Scientific, Fair Lawn, NJ). When fluorescently labelled secondary antibodies were used, sections were counterstained with Thioflavin S (Sigma, St. Louis, MO) 0.05% in 50% ethanol for 8 min and coverslipped with Vectashield® mounting media with 4′,6-diamidino-2-phenylindole (DAPI; Vector Lab., Burlingame, CA).

Amyloid load and amyloid plaque size distribution

Amyloid load was measured as the percent of total surface stained for Aβ by 10D5 antibody (Elan Pharmaceuticals, Inc.) in sections counterstained with haematoxylin and periodic acid–Schiff base method (for vascular basement membranes). Sections were imaged on an upright Leica DMRB microscope equipped with a motorized stage and a CCD camera (model DC330, DAGE-MTI, Inc. Michigan City, IN), and coupled with the BIOQUANT NOVA PRIME software (version 6.90.10, MBSR, Nashville, TN). Amyloid load was measured in three anatomical regions: the molecular layer of the dentate gyrus, CA1 and subiculum-presubiculum. Plaque and vascular amyloid loads were determined separately in order to detect a potential shift of the amyloid from plaques to blood vessel walls. The size distribution of the amyloid plaques was also measured.

Stereology-based studies

Stereological studies were performed using an Olympus BX51 upright microscope (Olympus, Tokyo, Japan) equipped with a motorized stage and an Olympus DP70 camera, and coupled with the CAST software (version 2.3.1.5). Densities of amyloid plaques and neurofibrillary tangles were quantified with the optical dissector technique as described previously (Hyman *et al*., 1998) in sections stained with thioflavin-S and immunostained either with 3D6 anti-Aβ antibody (Elan Pharmaceuticals, Inc) or with the anti-tau antibodies paired helical filament (PHF)-1 or Alz50 (both kind gifts from Dr Peter Davies). Coefficient errors were calculated in preliminary studies to obtain appropriate sampling fractions. The regions of the hippocampus (granular layer of the dentate gyrus, molecular layer of the dentate gyrus, CA1 and subiculum-presubiculum) were outlined under the 4× objective and randomly sampled under the 20× objective, typically with a 10% sampling fraction. PHF1, Alz50 and thioflavin-S positive neurons were counted in the granular layer of the dentate gyrus, CA1 and subiculum-presubiculum with a counting frame of 5% (7130 μm^2). Amyloid plaques (3D6-immunoreactive and thioflavin-S positive) were counted in the molecular layer of the dentate gyrus, CA1 and subiculum-presubiculum with a counting frame of 10% (14 261 μm^2). Dense-core plaques immunoreactive for the mitochondrial marker

Table 1 Baseline characteristics of study subjects

	Non-demented controls ($n = 8$)	Non-immunized patients ($n = 13$)	AN1792-treated patients ($n = 5$)	*P* value
Age, years (mean ± SD)	82.7 ± 10.7	77.4 ± 7.3	78.6 ± 5.9	NS
Gender, *n* (% female)	4 (50)	8 (61.5)	2 (40)	NS
Duration of disease, years (mean ± SD)	NA	10.0 ± 4.5	8.4 ± 3.5	NS
Post-mortem interval, h (mean ± SD)	21.6 ± 13.8	12.7 ± 5.3	21.2 ± 29.9	NS
ApoE genotype:				
ApoE4 carriers, *n* (%)	2 (25)	10 (76.9)	3 (60)	0.0318[a]
ApoE4 alleles, *n* (%)	2 (12.5)	13 (50)	3 (30)	0.0203[a]

NA = not applicable; NS = non significant.
a Differences were significant only between non-demented controls and non-immunized patients (χ^2 with Fisher's exact test).

voltage-dependent anion-selective channel protein 1 (VDAC1) (porin, Abcam, ab15895) were counted in these same regions with a 20% sampling fraction and a counting frame of 10% (14 261 μm^2).

Curvature ratio analysis

Neurites were identified by immunohistochemistry directed against neurofilament heavy chain (Abcam, ab40796) and sections were counterstained with thioflavin-S and DAPI prior to imaging in the manner described above for stereologic measurements. The hippocampal regions were outlined with the CAST software under the 4× objective of the microscope, and randomly sampled under the 20× objective, with the following sampling fractions: 25% in the molecular layer of the dentate gyrus, 15% in the CA1 and 15% in the subiculum-presubiculum. Pictures were coded and stored in a blinded manner prior to analysis with ImageJ (http://rsbweb.nih.gov/ij/download.html). Neurite segments identified by the presence of neurofilament heavy chain were numbered, and their lengths measured by an observer blinded to the condition of the subject or the presence of dense-core plaques in the field under study. Curvature ratio of each neurite segment was calculated as the ratio of measured length to the end-to-end length of the same neurite; thus, increased neurite curvature results in a higher curvature ratio (Knowles *et al.*, 1999). Only segments with a measured length longer than 20 μm were included in the analyses. The number of 20 × hippocampal fields analysed was not significantly different across groups [214 fields in 8 non-demented controls (mean ± SEM; 26.7 ± 2.6), 388 in 13 non-immunized patients with Alzheimer's disease (29.7 ± 2.1) and 122 in 4 immunized patients with Alzheimer's disease (30.5 ± 3.9)]. The neurofilament heavy chain immunohistochemistry was not feasible in one of the immunized cases.

To address the relationship between neurite curvature and their proximity to dense-core plaques, the curvature ratio analysis was focused on the CA1 subfield. 100% of CA1 was sampled and pictures of fields containing dense-core plaques were coded and stored in separate folders for neurofilament heavy chain and thioflavin-S images. Using ImageJ, dense-core plaques in the thioflavin-S pictures were outlined and transferred to the corresponding neurofilament heavy chain images. The curvature ratio of neurite segments within 50 μm from the dense-core plaques edge was compared with the curvature ratio of neurite segments located beyond this boundary (i.e. either in previous pictures containing dense-core plaques or in pictures lacking them). The distance of neurite segments to dense-core plaques edge was calculated as the average of three distances: distances from the nearest plaque edge to each end of the neurite segment as well as the distance from the plaque edge to the midpoint of the neurite segment.

Number of dystrophic neurites per plaque

To identify dystrophic neurites around dense-core plaques, immunohistochemistry was performed with SMI312 antibody (Covance, SMI-312R), followed by thioflavin-S and DAPI counterstaining. Hippocampal regions were outlined with the CAST software under the 4 × objective as described previously. 100% of the molecular layer of the dentate gyrus, CA1, and subiculum-presubiculum was sampled under the 20× objective. Images of fields containing dense-core plaques were coded and stored in a blind fashion and analysed with ImageJ software. Dense-core plaques in the thioflavin-S pictures were outlined and transferred to the corresponding SMI312 pictures. Dystrophic neurites and varicosities/swellings either embedded or in contact with the thioflavin-S positive area were counted manually.

Number of reactive astrocytes per plaque

To visualize reactive astrocytes around dense-core plaques immunohistochemistry with a glial fibrillar acid protein antibody (Sigma, G9269) was done, followed by thioflavin-S and DAPI counterstaining. The same protocol as for SMI312-positive dystrophic neurites was followed, except that glial fibrillar acid protein and thioflavin-S pictures of the same fields were merged with the appropriate tool in ImageJ software. Reactive astrocytes with a visible nucleus by DAPI staining surrounding dense-core plaques as far as 50 μm from the plaques edge were manually counted. Reactive astrocytes located close to two or more dense-core plaques (i.e. within 50 μm) were 'split' among those plaques (i.e. 0.5 astrocytes for those close to two plaques, 0.33 for those close to three plaques and 0.25 for those close to four plaques). This conservative method was implemented to avoid double-counting of astrocytes per plaque in areas with high density of dense-core plaques, a situation that would be presumably more common in non-immunized Alzheimer's disease patients and might otherwise bias the results.

Statistical analysis

All statistical analyses were conducted with the statistical package PRISM Graph Pad for Mac (version 5.0). Normality of datasets was assessed with Kolmogorov–Smirnov and Schapiro–Wilk tests. Non-normal measures included the size of total amyloid plaques and dense-core plaques, neurite curvature ratio, number of dystrophic neurites per plaque and number of astrocytes per plaque. For these data, results are expressed as median (interquartile range). A non-parametric one-way ANOVA (Kruskal–Wallis) with Dunn's multiple comparison post-test was used for all-group comparisons and a non-parametric two-tailed *t*-test (Mann–Whitney, *U*) was run for pairwise comparisons. Normal data included amyloid load, densities of total amyloid plaques and dense-core plaques, and densities of PHF1, Alz50 and thioflavin-S positive neurons. For these, results are expressed as mean ± SEM. All-group comparisons were performed with a parametric one-way ANOVA with Bonferroni correction, and pairwise comparisons were done with a parametric two-tailed *t*-test with Welch's correction when variances were significantly different between groups. Pairwise comparisons between proportions were performed with χ^2 with Fisher's exact test. Correlations were carried out with the Pearson's statistic if both datasets were normally distributed or with the Spearman's rank test if one or both datasets were not normal. The level of significance was set at $P < 0.05$.

Results

Baseline characteristics

Baseline characteristics of the three groups are listed in Table 1 and Supplementary Table 1. Additional characteristics of the immunized patients with Alzheimer's disease can be found in Table 2 and Supplementary Table 2. Non-demented controls and non-immunized and immunized patients with Alzheimer's disease were matched by age and gender. These two latter groups

Table 2 Additional characteristics of AN1792-treated patients in this study

Subject	Number of doses	Antibody titres	Survival after first dose (months)	Reference
22	2	IgG+	15	Ferrer *et al*. 2004
23	3	1:2771	12	Masliah *et al*. 2005
24	2	Not detectable	40	Uro-Coste *et al*. 2010
25	2	TAPIR 1/4	46	Unpublished
26	2	IgM > 1:3500 IgG > 10 000	34	Bombois *et al*. 2007

TAPIR = tissue amyloid plaque immunoreactivity assay. A score of 1 (out of 4) denotes weak staining of amyloid plaques in immunohistochemical brain sections of $APP^{swe} \times PS1^{M146L}$ double transgenic mice with the patient's serum.

were also matched for Braak stage of neurofibrillary tangles and did not differ in terms of disease duration or *ApoE* genotype. Post-mortem interval was not significantly different across groups. The detailed results of each case for the main quantitative analyses are shown in Supplementary Table 4.

Amyloid load and density of amyloid plaques

Plaque and vascular amyloid loads were measured as the percent of total surface stained by 10D5 anti-Aβ antibody in the neuropil and vessels of hippocampal sections counterstained with haematoxylin and periodic acid-Schiff. Plaque amyloid load in the hippocampus was significantly different across the three groups (ANOVA, $F = 15.11$, $P < 0.0001$) (Fig. 1A, Supplementary Fig. 1). As expected, hippocampal plaque amyloid load was significantly higher in non-immunized Alzheimer's disease patients than in non-demented controls ($0.700 \pm 0.098\%$ versus $0.080 \pm 0.050\%$, $t = 5.588$, $df = 17$, $P < 0.0001$). Plaque amyloid load in the immunized Alzheimer's disease patients was significantly lower than that in the non-immunized patients ($0.146 \pm 0.069\%$ versus $0.700 \pm 0.098\%$, $t = 3.315$, $df = 16$, $P = 0.0044$); in fact, the load in these treated subjects was not different from age-matched non-demented controls ($0.146 \pm 0.069\%$ versus $0.080 \pm 0.050\%$, $t = 0.7781$, $df = 11$, $P = 0.4529$). No vascular amyloid was detected in non-demented controls. Hippocampal vascular amyloid load in immunized patients did not differ significantly from non-immunized patients ($0.013 \pm 0.005\%$ versus $0.026 \pm 0.008\%$, $t = 0.8895$, $df = 16$, $P = 0.3869$) (Fig. 1B).

Densities of total and dense-core plaques were quantified with an unbiased stereological approach in hippocampal sections double-stained with 3D6 anti-Aβ antibody and thioflavin-S (Fig. 1C–D). There were significant differences across groups in the densities of 3D6 (total) and of thioflavin-S positive (dense-core) plaques (ANOVA, $F = 34.68$ and 27.06, respectively, $P < 0.0001$ for both comparisons). As expected, non-immunized Alzheimer's disease patients had a density of both total and dense-core amyloid plaques significantly higher than non-demented controls (3D6: 22.07 ± 1.956 plaques/mm^2 versus 1.738 ± 0.970 plaques/mm^2, $t = 9.311$, $df = 16$, $P < 0.0001$; thioflavin-S: 16.17 ± 1.570 plaques/mm^2 versus 1.408 ± 0.788 plaques/mm^2, $t = 8.399$, $df = 16$, $P < 0.0001$). By contrast, AN1792-treated patients had a density of total and dense-core amyloid plaques significantly lower than non-immunized patients (3D6: 4.566 ± 2.799 plaques/mm^2 versus 22.07 ± 1.956 plaques/mm^2, $t = 4.846$, $df = 16$, $P = 0.0002$; thioflavin-S: 4.102 ± 2.349 plaques/mm^2 versus 16.17 ± 1.570 plaques/mm^2, $t = 4.122$, $df = 16$, $P = 0.0008$) and not significantly different from non-demented controls (3D6: 4.566 ± 2.799 plaques/mm^2 versus 1.738 ± 0.970 plaques/mm^2, $t = 1.137$, $df = 11$, $P = 0.2796$; thioflavin-S: 4.102 ± 2.349 plaques/mm^2 versus 1.408 ± 0.788 plaques/mm^2, $t = 1.087$, $df = 4$, $P = 0.3381$). A sub-regional analysis revealed significant differences between both Alzheimer's disease groups in all the hippocampal regions analysed (data not shown).

We also calculated the proportion of dense-core plaques among the total amyloid plaques in each group using the same sections double-stained with 3D6 and thioflavin-S and the raw data obtained with the quantification above (Fig. 1E). This proportion was significantly different across groups ($\chi^2 = 22.30$, $df = 2$, $P < 0.0001$; χ^2 for trend $= 8.499$, $df = 1$, $P = 0.0036$). Pairwise comparisons revealed that the immunized group had a significantly higher proportion of dense-core plaques than the non-immunized Alzheimer's disease cases (89.09% versus 72.89%, Fisher's exact test, $P < 0.0001$). Non-demented controls had a proportion of dense-core plaques intermediate between non-immunized and immunized patients, but not significantly different from them (82.26% versus 72.89%, Fisher's exact test, $P = 0.1082$ and 82.26% versus 89.09%, Fisher's exact test, $P = 0.1840$, respectively). A comparison of the correlation between density of total and dense-core amyloid plaques in both Alzheimer's disease groups also revealed the overwhelming predominance of the dense-core type of amyloid plaques in the immunized group ($r = 0.9990$, $P < 0.0001$ in the immunized group versus $r = 0.6624$, $P = 0.0136$ in the non-immunized group; Pearson's correlation test) (Fig. 1F).

The size of total amyloid plaques was measured in 10D5-immunostained sections and that of dense-core plaques was measured in thioflavin-S stained sections. Both total and dense-core amyloid plaques were significantly smaller in immunized patients with respect to non-immunized patients (Fig. 1G–H, Supplementary Fig. 2A–B) [total amyloid plaques: 197.1 (98.88–404.7) μm^2 versus 261.1 (126.6–638.3) μm^2, $U = 1039\,000$, $P < 0.0001$; dense-core plaques: 930.7 (555.2–1565) μm^2 versus 1181 (753.4–1974) μm^2, $U = 119\,700$, $P < 0.0001$]. No significant differences were found in the size of both total and dense-core amyloid plaques between the

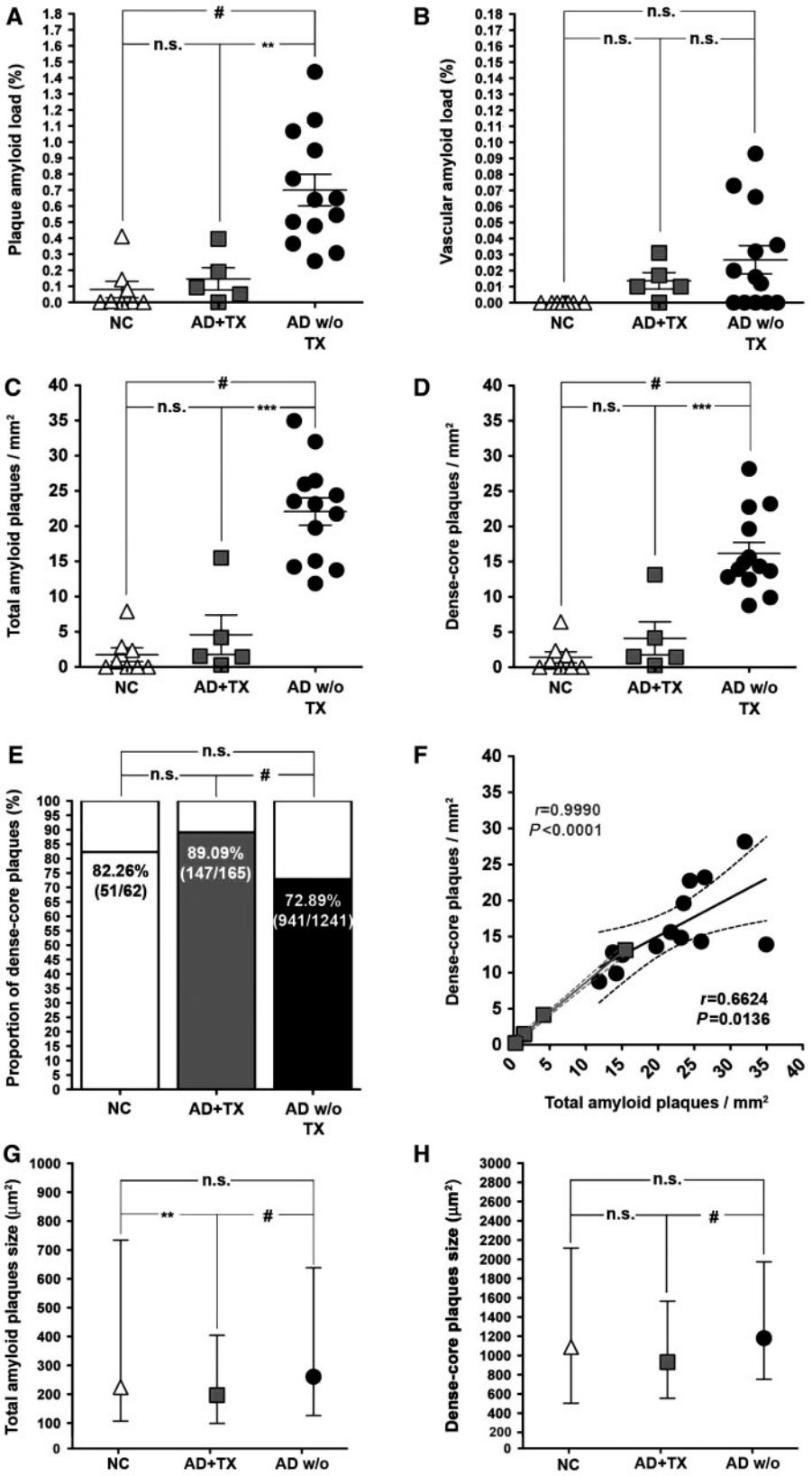

Figure 1 Decreased hippocampal amyloid deposition after anti-Aβ immunization. Plaque amyloid load in AN1792-treated Alzheimer's disease patients is reduced down to the levels of non-demented controls (NC) (**A**), without significant increase of vascular amyloid load (**B**). Density of both total amyloid plaques (**C**) and dense-core plaques (**D**) is significantly decreased in the immunized group. Bars in scatter-dot plots **A–D** denote mean ± SEM. Two-tailed unpaired *t*-tests were run for these pairwise comparisons (n.s. = non-significant; $^{**}P<0.01$; $^{***}P<0.001$; $^{\#}P<0.0001$). (**E**, **F**) The proportion of dense-core plaques is significantly increased after immunization. In **E**, the

Continued

non-immunized Alzheimer's disease group and the non-demented group [total amyloid plaques: 261.1 (126.6–638.3) μm^2 versus 224.5 (107–734.3) μm^2, $U = 437\,100$, $P = 0.5765$; dense-core plaques: 1181 (753.4–1974) μm^2 versus 1089 (503.9–2117) μm^2, $U = 27\,460$, $P = 0.6599$]. Lastly, total amyloid plaques were also significantly smaller in the immunized group compared to non-demented controls, but this difference did not reach statistical significance for dense-core plaques [total amyloid plaques: 197.1 (98.88–404.7) μm^2 versus 224.5 (107–734.3) μm^2, $U = 61\,760$, $P = 0.0062$; dense-core plaques: 930.7 (555.2–1565) μm^2 versus 1089 (503.9–2117) μm^2, $U = 6894$, $P = 0.1575$].

Analysis of neurite curvature ratio

Neurite curvature ratio was measured in sections immunostained with an anti-neurofilament heavy chain antibody and counterstained with thioflavin-S and DAPI.

When considering neuritic curvature independent of the distance to dense-core plaques, there was a significant positive correlation between the median curvature ratio and density of both total amyloid plaques and dense-core plaques in the non-immunized Alzheimer's disease group (total amyloid plaques: $r = 0.7692$, $P = 0.0021$; for dense-core plaques: $r = 0.5714$, $P = 0.0413$, Spearman's rank test) (Fig. 2A–B). There were statistically significant differences in the curvature ratio across the three groups of subjects (Kruskal–Wallis ANOVA = 84.73, $P < 0.0001$). As expected, the curvature ratio was abnormally higher in non-immunized Alzheimer's disease patients compared to non-demented controls [1.027 (1.014–1.047) versus 1.020 (1.010–1.037), $U = 1129\,000$, $P < 0.0001$]. Importantly, the curvature ratio was significantly lower in immunized compared to non-immunized patients [1.021 (1.010–1.041) versus 1.027 (1.014–1.047), $U = 567\,400$, $P < 0.0001$], reaching a value not different from non-demented controls [1.021 (1.010–1.041) versus 1.020 (1.010–1.037), $U = 339\,700$, $P = 0.0960$] (Fig. 2C, Supplementary Fig. 2C).

We then examined the influence of the proximity to dense-core plaques on the curvature ratio, performing the analysis in a plaque-based rather than in a random fashion, focusing on the CA1 subfield (Fig. 2D). As expected, in the non-immunized Alzheimer's disease group, the curvature ratio was significantly higher close to the plaques ($<50\,\mu m$) than far away from them ($\geq 50\,\mu m$) [1.043 (1.023–1.075) close versus 1.028 (1.015–1.049) far, $U = 453\,600$, $P < 0.0001$]. Conversely, in the immunized group both curvature ratio values close to and far from the dense-core plaques were almost identical [1.022 (1.009–1.038) close versus 1.020 (1.010–1.036) far, $U = 40\,570$, $P = 0.5641$]. Moreover, both curvature ratio values in the immunized group were significantly lower than the corresponding curvature ratio values in the non-immunized group (close: $U = 117\,200$, $P < 0.0001$; far: $U = 100\,800$, $P < 0.0001$). Importantly, in neither of the Alzheimer's disease groups was the curvature ratio of neurites close to plaques influenced by the size of the plaques (Kruskal–Wallis ANOVA with Dunn's multiple comparison post-test: $P > 0.05$), whereas the significant difference observed in the curvature ratio close to plaques between both Alzheimer's disease groups was preserved across different plaque size intervals (Kruskal–Wallis ANOVA with Dunn's multiple comparison post-test: $P \leq 0.001$, except for the plaque size interval 1500–2000 μm^2, which did not reach significance, probably due to the small number of neurites measured close to plaques of this size in the immunized group, $n = 18$) (Fig. 2E).

Dystrophic neurites/varicosities per dense-core plaque

Dystrophic neurites and axonal swellings or spheroids per dense-core plaque were counted within the thioflavin-S positive area in sections stained with SMI312 antibody and counterstained with thioflavin-S. Dense-core plaques in non-immunized Alzheimer's disease patients had significantly more dystrophic neurites compared to plaques in non-demented controls [2 (1–4) dystrophies/plaque versus 1 (0–3) dystrophy/plaque, $U = 20\,790$, $P = 0.0007$]. Unexpectedly, there was a significant increase in the number of dystrophic neurites per dense-core plaque in the immunized patients compared to non-immunized patients [4 (2–6) dystrophies/plaque versus 2 (1–4) dystrophies/plaque, $U = 116\,800$, $P < 0.0001$] (Fig. 3A, Supplementary Fig. 2D).

Proportion of VDAC1-immunoreactive dense-core plaques

Accumulation of mitochondria in dystrophic neurites of dense-core plaques was examined by immunohistochemistry for the outer mitochondrial membrane marker VDAC1 with thioflavin-S counterstaining. The proportion of dense-core plaques immunoreactive for VDAC1 in non-immunized Alzheimer's disease patients was higher than that in non-demented controls, although this

Figure 1 Continued
bar graph shows total amyloid plaques counted on sections immunostained for 3D6 anti-Aβ antibody normalized to 100%. Filled bars represent the percent of amyloid plaques co-stained with thioflavin-S (dense-core plaques). Raw fractions are presented in parenthesis within the filled bars, with the number of total amyloid plaques counted in the denominator and the number of dense-core plaques in the numerator. In **F**, the correlation between total amyloid plaques and dense-core plaques in both Alzheimer's disease groups is shown. Pairwise comparisons in **E** were done with χ^2 with Fisher's exact test ($^{\#}P < 0.0001$), whereas correlations in **F** were performed with Pearson's test. (**G**, **H**) Remaining total amyloid plaques and dense-core plaques in immunized patients are significantly smaller compared to plaques in non-immunized patients, whereas their size does not differ between non-immunized patients and non-demented controls. Single-symbol plots in **G** and **H** represent median values, whereas bars denote interquartile ranges. These pairwise comparisons were performed with a Mann–Whitney test ($^{**}P < 0.01$, $^{\#}P < 0.0001$). Automatic measurement of total amyloid plaques size included 225 plaques from non-demented controls (NC), 626 plaques from immunized patients (AD + TX) and 3973 plaques from non-immunized patients (AD w/o TX). Manual measurement of dense-core plaques size was performed on 55 plaques from non-demented controls, 285 plaques from immunized patients and 1035 plaques from non-immunized patients.

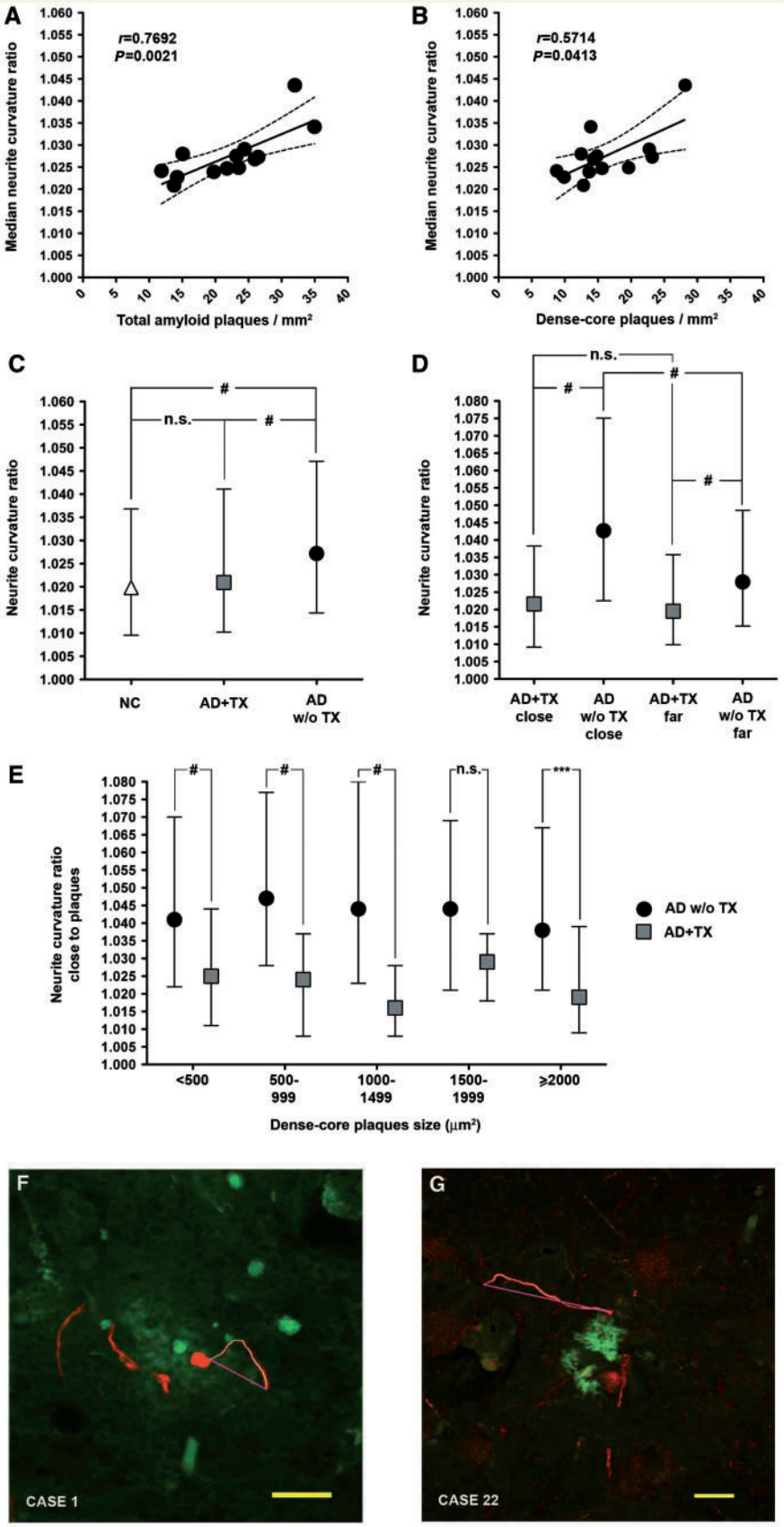

Figure 2 Improvement of neurite trajectories in immunized patients with Alzheimer's disease. (**A**, **B**) Neurite curvature ratio correlates significantly with the density of total and dense-core amyloid plaques in non-immunized patients with Alzheimer's disease. Correlations were performed with Spearman's rank test. Dotted lines represent the 95% confidence intervals. (**C**) Neurite trajectories in the

Continued

difference did not reach statistical significance (38.96% versus 31.43%, respectively, Fisher's exact test, $P = 0.4771$). Remarkably, more than half (56.25%) of the dense-core plaques in the AN1792-treated patients were VDAC1-positive, a proportion significantly higher compared to the other two groups ($P = 0.0009$ versus non-immunized group; $P = 0.0121$ versus non-demented group, Fisher's exact test) (Fig. 3B).

Reactive astrocytes per dense-core plaque

We counted the number of glial fibrillar acid protein-positive reactive astrocytes per dense core-plaque (up to 50 μm from the edge of the plaque) in sections counterstained with thioflavin-S. Dense-core plaques had a more severe astrocytosis in non-immunized Alzheimer's disease patients than that in non-demented controls [1.5 (0.4575–3) astrocytes/plaque versus 0.33 (0–1.040) astrocytes/plaque, $U = 22\,070$, $P < 0.0001$]. The extent of astrocytosis surrounding dense-core plaques remaining after immunization was slightly but not significantly decreased, when compared to plaques from non-immunized patients with Alzheimer's disease [1 (0–3) astrocyte/plaque versus 1.5 (0.4575–3) astrocytes/plaque, $U = 73\,110$, $P = 0.6060$], but still more severe than that around dense-core plaques from non-demented controls ($U = 3548$, $P = 0.0006$) (Fig. 3C, Supplementary Fig. 2E).

Alterations in neuronal tau

To analyse the amount of abnormal neuronal tau quantitatively, we performed immunohistochemical studies with two different anti-tau antibodies: the phosphorylation-dependent antibody PHF1 to assess the phosphorylation status of tau and the conformation-dependent antibody Alz50 to evaluate the misfolding status of tau (Fig. 4A–B). The density of thioflavin-S positive neurofibrillary tangles (i.e. tau fibrillar aggregates with a β-sheet conformation) was also quantitated in a stereological fashion (Fig. 4C).

As expected, densities of Alz50-positive and PHF1-positive neurons and thioflavin-S positive neurofibrillary tangles were significantly higher in non-immunized Alzheimer's disease patients (Braak stages IV–VI) than in non-demented controls (Braak stages I–III) (Alz50: 16.08 ± 2.534 neurons/mm^2 versus 6.948 ± 2.915 neurons/mm^2, $t = 2.305$, $df = 19$, $P = 0.0326$; PHF1: 47.44 ± 6.138 neurons/mm^2 versus 5.464 ± 2.042 neurons/mm^2, $t = 6.489$, $df = 14$, $P < 0.0001$; thioflavin-S: 34.12 ± 6.990 neurofibrillary tangles/mm^2 versus 4.468 ± 1.885 neurofibrillary tangles/mm^2, $t = 4.096$, $df = 13$, $P = 0.0013$). Of note, immunized patients showed a significant reduction in the density of PHF1-positive neurons compared to non-immunized patients, despite being matched for the Braak stage (18.53 ± 10.49 neurons/mm^2 versus 47.44 ± 6.138 neurons/mm^2, $t = 2.445$, $df = 16$, $P = 0.0264$) (Figs 4A and 4E–L). No difference was found in the densities of Alz50-positive neurons and thioflavin-S positive neurofibrillary tangles between the Alzheimer's disease groups (Alz50: 17.42 ± 9.152 neurons/mm^2 in AN1792-treated versus 16.08 ± 2.534 neurons/mm^2 in non-treated, $t = 0.1407$, $df = 4$, $P = 0.8949$; thioflavin-S: 18.56 ± 7.690 neurofibrillary tangles/mm^2 in AN1792-treated versus 34.12 ± 6.990 neurofibrillary tangles/mm^2 in non-treated, $t = 1.261$, $df = 16$, $P = 0.2255$). A correlation between densities of PHF1-positive and Alz50-positive neurons for both Alzheimer's disease groups revealed a predominance of PHF1-positive over Alz50-positive neurons in non-immunized patients with Alzheimer's disease whereas both densities were similar in the immunized group ($r = 0.3899$, $P = 0.1878$, in the non-immunized group, versus $r = 0.9755$, $P = 0.0046$, in the immunized group, Pearson's correlation test) (Fig. 4D).

Discussion

Successful removal of hippocampal amyloid

Both active and passive immunotherapy against Aβ peptide have been shown to clear amyloid plaques or prevent Aβ deposition in

Figure 2 Continued
hippocampus of immunized patients are significantly straighter compared to non-immunized patients and similar to non-demented controls. Curvature ratio was analysed in 1231 neurites from 8 normal controls, 580 neurites from 4 immunized patients and 2243 neurites from 13 non-immunized patients. In one of the immunized cases an appropriate neurofilament heavy chain immunostaining was not feasible, probably due to differences in fixation protocols. (**D**) Improvement of curvature ratio in immunized patients is not only attributable to a lower plaque load but also occurs within the vicinity (<50 μm) of remaining dense-core plaques. Curvature ratio was determined in 321 neurites close to and 260 neurites far from plaques in the immunized group, and in 1256 neurites close to and 972 neurites far from plaques in the non-immunized group. Pairwise comparisons in **C** and **D** were performed with Mann–Whitney test ($^{\#}P < 0.0001$). (**E**) Curvature ratio of neurites close to plaques is not simply due to a 'mass effect' caused by the plaques because plaque size does not affect the curvature ratio of surrounding neurites (within-group comparisons were not significant but are not illustrated for clarity purposes). Moreover, the improvement of the curvature ratio close to plaques in the immunized subjects is not explained by the smaller size of their plaques because between-group significant difference is preserved across different plaque size intervals. This analysis included 143, 281, 202, 171 and 276 neurites close to plaques of increasing size intervals from the non-immunized Alzheimer's disease subjects, and 112, 59, 41, 18 and 50 neurites close to plaques of the same size intervals from the AN1792-treated Alzheimer's disease subjects. A Kruskal–Wallis ANOVA with Dunn's multiple comparison post-test was run ($^{***}P < 0.001$, $^{\#}P < 0.0001$, n.s. = non significant). (**F, G**) Representative pictures of neurite segments within the vicinity of a dense-core plaque in the CA1 region of a non-immunized patient with Alzheimer's disease (**F**, Case 1), and an AN1792-treated patient with Alzheimer's disease (**G**, Case 22). Neurites were immunostained with a neurofilament heavy chain antibody (in red) and plaques were stained with thioflavin-S (in green). Neurite curvature ratio was calculated as the ratio of the measured length (white line) to the end-to-end length (pink line). Compare the abnormally curve trajectory of neurites in **F** with the straighter trajectory of neurites in **G**. Scale bars = 20 μm. NC = non-demented controls; AD + TX = plaques from immunized patients; AD w/o TX = non-immunized patients.

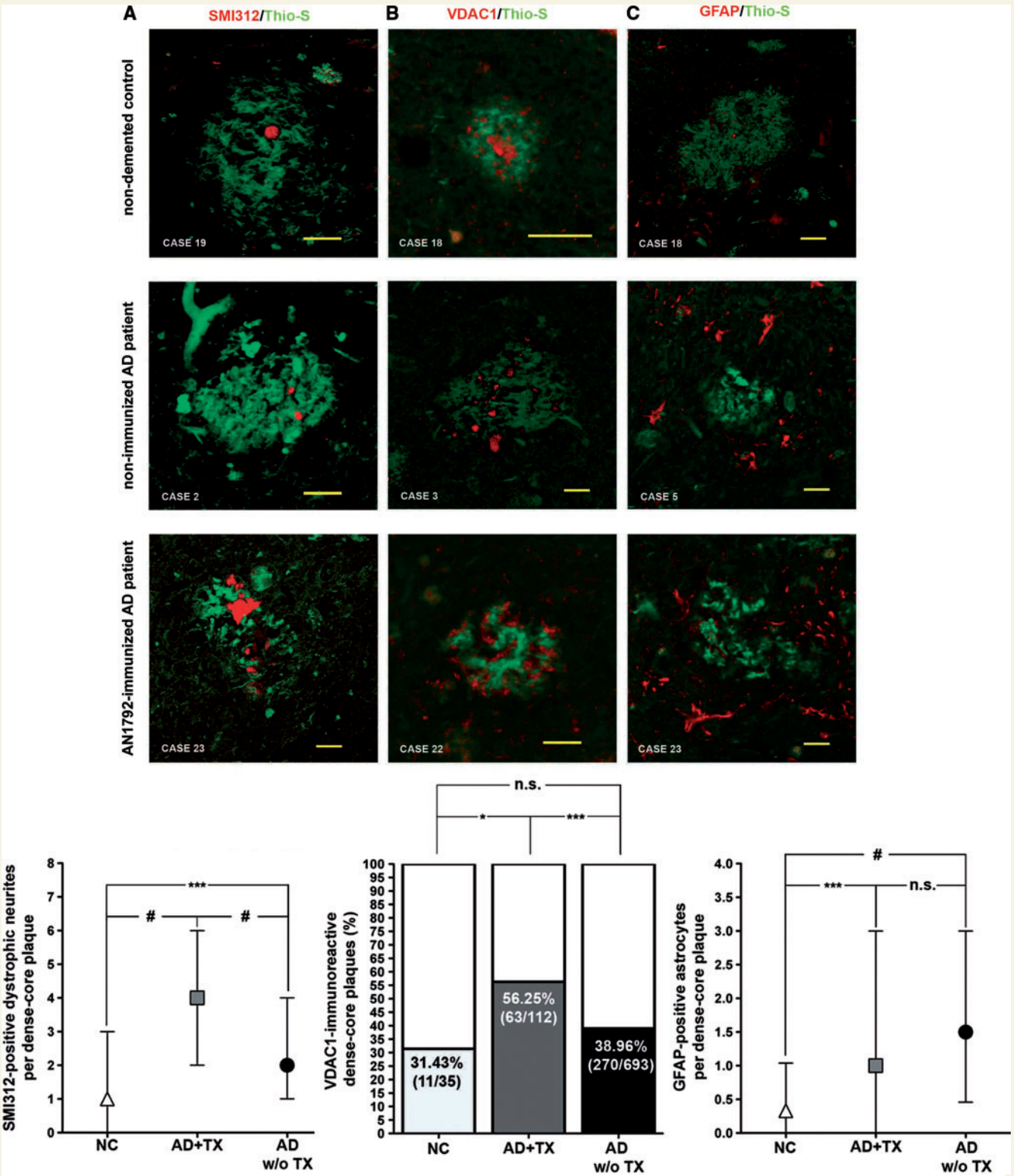

Figure 3 Dense-core plaques remaining after immunization retain some of their toxic properties. (**A**) Representative images of dense-core plaques (in green) from a non-demented control (Case 19), a non-immunized patient (Case 2) and an AN1792-treated patient (Case 23), with the neurofilament antibody SMI312 depicting associated dystrophic neurites and axonal varicosities or swellings (in red). Quantification of the number of dystrophic neurites and varicosities per plaque yielded a significant increase in the amount of neuritic dystrophy in the remaining plaques of immunized patients, as compared to non-immunized patients. Pairwise comparisons were done with the Mann–Whitney test [$^{***}P<0.001$, $^{\#}P<0.0001$; $n=55$, 285 and 1035 plaques in normal controls (NC), immunized patients (AD + TX) and non-immunized patients (AD w/o TX), respectively]. (**B**) Representative images of mitochondria accumulation in dense-core plaques associated-dystrophic neurites from a non-demented control (Case 19), a non-immunized patient (Case 3) and an

Continued

several mouse models of Alzheimer's disease (Schenk *et al.*, 1999; Bard *et al.*, 2000; Morgan *et al.*, 2000; Janus *et al.*, 2000; Bacskai *et al.*, 2001, 2002; DeMattos *et al.*, 2001; Lemere *et al.*, 2003; Wilcock *et al.*, 2004). Post-mortem studies of brain specimens from participants in the Phase 2a active immunization trial also revealed a significant decrease in amyloid pathology, as measured with either amyloid load or density of amyloid plaques per field (Nicoll *et al.*, 2003; Ferrer *et al.*, 2004; Masliah *et al.*, 2005; Bombois *et al.*, 2007; Holmes *et al.*, 2008).

Our results are in agreement with these previous autopsy reports. Compared to the hippocampus of non-immunized patients from our brain bank, the hippocampus of this subset of immunized Alzheimer's disease patients had a significantly lower amount of amyloid deposits, as measured in sections stained with the 10D5 antibody, an antibody that recognizes the N-terminus of the Aβ peptide. Indeed, active immunization reduced the hippocampal plaque amyloid load in the treatment group down to the levels existing in age-matched non-demented controls. The same result was achieved after the stereological quantification of density of amyloid plaques in sections stained with the 3D6 antibody, which also binds to the N-terminus of the Aβ peptide. Since anti-Aβ antibodies generated after AN1792 immunization are mainly directed against the N-terminus of the Aβ peptide (Lee *et al.*, 2005), the results herein could be explained by a competition between 10D5 and 3D6 antibodies and *de novo* endogenous anti-Aβ antibodies to bind amyloid plaques. However, stereological quantification of plaques in thioflavin-S stained sections also yielded similarly lower density of dense-core plaques in immunized patients, ruling out this possibility.

Interestingly, our quantitative analysis revealed a significantly higher proportion of dense-core plaques among the remaining amyloid plaques in the immunized cases, as compared to non-immunized Alzheimer's disease cases. A sub-regional analysis showed that this difference was mainly driven by the stereological quantification in the subiculum-presubiculum (data not shown). Indeed, the hippocampal sections from four out of the five immunized Alzheimer's disease patients were virtually devoid of the confluent, diffuse, 'cloud-like' amyloid deposits, typically seen in the parvopyramidal layer of the presubiculum (see Supplementary Fig. 1) (Kalus *et al.*, 1989; Akiyama *et al.*, 1990; Wisniewski *et al.*, 1998). Thus, these data indicate that AN1792 immunization was comparatively more effective at clearing diffuse amyloid deposits than dense-core plaques.

We compared the size distribution of amyloid plaques in hippocampal sections from the three groups of subjects and found that both total amyloid plaques and dense-core plaques were significantly smaller in immunized patients, with respect to non-immunized patients and non-demented controls. Despite the static nature of any post-mortem study, this result is consistent with the *in vivo* observation of a reduction in dense-core plaques size after topical administration of anti-Aβ antibodies in an Alzheimer's disease mouse model (Bacskai *et al.*, 2002). This observation, together with the relative abundance of collapsed 'moth-eaten' plaques remaining after AN1792 immunization already noted in previous post-mortem reports (Nicoll *et al.*, 2003; Ferrer *et al.*, 2004), also points towards a sequential pattern of amyloid removal: plaques halo, containing more soluble amyloid species, would be removed more readily, whereas insoluble amyloid fibrils compactly packed within the plaque core would be harder to solubilize.

According to previous reports, amyloid removal seems to be proportional to the immunological response to AN1792 as measured with antibody titres in plasma or CSF (Holmes *et al.*, 2008). Of note, in our study, both an antibody responder patient who developed a subacute meningoencephalitis and a patient with undetectable antibody titres by enzyme-linked immunosorbent assay had the highest amyloid loads and densities of dense-core plaques among the immunized patients.

A recent post-mortem study of eight other AN1792-immunized patients showed an overall increase in the extension and severity of cerebral amyloid angiopathy, suggesting that amyloid peptide is cleared through the vessels wall and efflux to the circulation (Boche *et al.*, 2008). Unlike this study, the clearance of amyloid plaques in the hippocampus of our subset of immunized patients was not translated into an increase of their vascular amyloid load, which was not significantly different from non-immunized patients. However, since cerebral amyloid angiopathy is usually more prominent in neocortical areas and our analysis was restricted to the hippocampus, we cannot rule out an overall increase of cerebral amyloid angiopathy in our immunized group.

Removal of amyloid plaques leads to recovery of neurite abnormal trajectories

We previously showed that the neurites within the dense-core amyloid plaques in the human Alzheimer's disease brain have a more abnormal trajectory compared to the neurites outside the

Figure 3 Continued
AN1792-treated patient (Case 22), as revealed by the mitochondrial marker VDAC1 (in red). Quantification of dense-core plaques immunoreactive for VDAC1 in the three study groups revealed an increase of the proportion of plaques VDAC1-positive in the immunized group, as compared to the non-immunized group. Dense-core plaques were normalized to 100% and filled bars represent the proportion of dense-core plaques immunoreactive for VDAC1. Raw fractions are shown in parenthesis within the filled bars, with the number of dense-core plaques counted in the denominator and the number of VDAC1-positive plaques in the numerator. Pairwise comparisons were done with χ^2 with Fisher's exact test ($^*P<0.05$, $^{***}P<0.001$). (**C**) Representative images of reactive astrocytosis surrounding dense-core plaques (in green) from a non-demented control (Case 18), a non-immunized patient (Case 5) and a patient treated with AN1792 (Case 23), as shown with a glial fibrillar acid protein immunostaining (in red). Quantification of the number of astrocytes per plaque resulted in a non-significant decrease of plaque-associated astrocytosis in the immunized group compared to the non-immunized patients. However, plaques from immunized patients still have more severe astrocytosis than plaques from non-demented controls. Pairwise comparisons were done with the Mann–Whitney test ($^{***}P<0.001$, $^{\#}P<0.0001$; $n=66$, 151 and 994 dense-core plaques, in the non-demented, immunized and non-immunized groups, respectively). Scale bars in **A–C** = 20 μm.

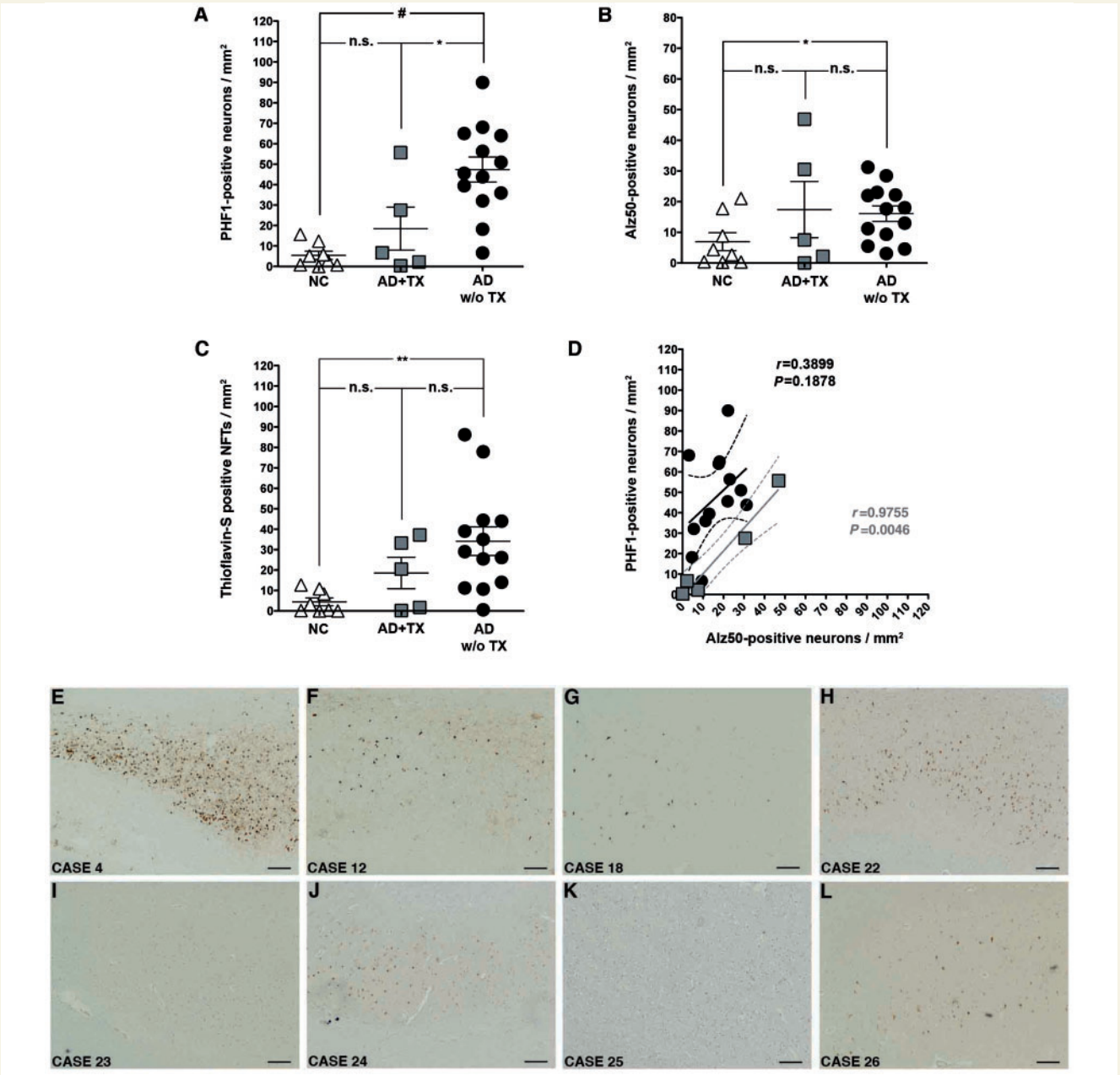

Figure 4 Decreased tau phosphorylation in neurofibrillary tangles after anti-Aβ immunization. (**A**) Hippocampal density of PHF1-positive neurons is significantly decreased in the immunized Alzheimer's disease patients compared to the patients with non-immunized Alzheimer's disease, despite both groups being matched for Braak stage. (**B**, **C**) No significant difference is observed in the densities of Alz50-positive neurons and thioflavin-S positive neurofibrillary tangles (NFT) between both Alzheimer's disease groups. Pairwise comparisons in **A–C** were done with a two-tailed *t*-test and bars represent mean ± SEM ($^{*}P<0.05$, $^{**}P<0.01$, $^{\#}P<0.0001$). (**D**) Correlations between densities of PHF1-positive neurons and Alz50-positive neurons in both Alzheimer's disease groups reveal a predominance of the late-stage phospho-tau species (PHF1) over the early-stage misfolded tau species (Alz50) in the non-immunized group. By contrast, neither of both tau epitopes is predominant in the Braak-matched immunized Alzheimer's disease group. Black circles represent each of non-immunized patients and grey squares represent immunized patients. Correlations were done with Pearson's test and dotted lines indicate the 95% confidence interval. For clarity purposes, non-demented controls are not represented. (**E–L**) Pictures show some of the PHF1-immunostained hippocampal sections used in the above analysis. The transition from the CA1 region to the subiculum (left-to-right in each picture) is illustrated for two representative non-immunized Alzheimer's disease patients (**E**, Case 4, Braak VI; and **F**, Case 12, Braak IV), one representative non-demented control (**G**, Case 18, Braak II) and the five AN1792-treated Alzheimer's disease patients (**H–L,** Cases 22–26). Scale bars = 200 μm.

plaques, and also compared to the neurites in the brain of non-demented controls (Knowles *et al.*, 1999). We also showed in Alzheimer's disease transgenic mouse models that the curvature ratio in neurites within 50 μm from the edge of the dense-core plaques is abnormally higher than the curvature ratio far away from this boundary (D'Amore *et al.*, 2003; Lombardo *et al.*, 2003; Spires-Jones *et al.*, 2009). In addition, *in vivo* imaging of the brain in one of these models revealed that changes in neurite trajectories follow the appearance of new plaques, arguing that this morphologic change is secondary to Aβ deposition (Meyer-Luehmann *et al.*, 2008). Lastly, passive immunotherapy in these Alzheimer's disease mouse models was able to normalize the curvature ratio of the neurites upon removal of amyloid plaques (Lombardo *et al.*, 2003; Spires-Jones *et al.*, 2009).

Based on this previous work in transgenic models of Aβ deposition, we analysed the curvature ratio of the neurites (dendrites and axons) in the hippocampus of the three groups of subjects and studied the influence of their proximity to dense-core plaques. The presence of a curvature ratio significantly higher in non-immunized Alzheimer's disease patients compared to non-demented controls confirmed the reproducibility and validity of this measure of neurite morphological abnormality. A subsequent analysis in the CA1 subfield with a plaque-based approach yielded a significantly higher curvature ratio of neurites located close to dense-core plaques (<50 μm), as compared to neurites far from them (≥ 50 μm), in non-immunized patients with Alzheimer's disease. This higher curvature ratio close to plaques was not influenced by the plaque size, supporting a local toxic effect of dense-core plaques on the trajectories of surrounding neurites rather than a 'mass effect', and further reinforcing the usefulness of this morphological measure. Examination of double-labelled hippocampal sections revealed that the 50 μm boundary around the edge of the thioflavin-S positive area was far away from the thin halo of more diffuse 3D6-positive but thioflavin-S-negative amyloid, also arguing against this 'mass effect' (results not shown).

Importantly, in the first of the two analyses, the neurite curvature ratio was significantly lower in AN1792-immunized patients than in non-immunized patients. Indeed, we observed an apparent normalization of this parameter of neuronal degeneration, since there was no significant difference between immunized patients and non-demented controls. This result is not merely due the existence of fewer plaques in the immunized Alzheimer's disease group, because in the plaque-based analysis performed subsequently, curvature ratios of both neurites located close to and far from dense-core plaques also were significantly lower in AN1792-treated patients, compared to the non-immunized patients. In fact, unlike these results in the non-immunized group, in the immunized patients both curvature ratios were almost identical. In addition, the significant difference observed in the curvature ratio close to plaques between both Alzheimer's disease groups is not merely due to the plaques from the immunized group being smaller and exerting less 'mass effect' on surrounding neurites; first, as mentioned above, the plaque size did not influence the curvature ratio of surrounding neurites, and second, the difference was preserved across different plaque size intervals. Thus, the significantly lower curvature ratio in the proximity of the remaining plaques in the AN1792 group unequivocally points to the reduction of an abnormal neurite morphology otherwise existing around the dense-core plaques.

Taken together, these results indicate that AN1792 immunization reproduces the beneficial effects on neurite trajectories observed with anti-Aβ passive immunization in preclinical studies (Lombardo *et al.*, 2003; Spires-Jones *et al.*, 2009) and further extend previous evidence of anti-Aβ immunization-induced improvement in markers of neuronal degeneration in the human Alzheimer's disease brain (Nicoll *et al.*, 2003; Ferrer *et al.*, 2004; Masliah *et al.*, 2005). While we have previously shown that plaque-induced neuritic curvature can potentially contribute to the cognitive deficits seen in Alzheimer's disease by disrupting the cortical synaptic integration (Knowles *et al.*, 1999; Stern *et al.*, 2004), the restoration of neurite trajectories observed in the hippocampus of this subset of immunized patients may not be sufficient to slow their cognitive decline (Supplementary Table 2) (Ferrer *et al.*, 2004; Masliah *et al.*, 2005; Bombois *et al.*, 2007; Uro-Coste *et al.*, 2010).

Toxic potential of amyloid plaques remaining after immunization

Passive anti-Aβ immunotherapy can promote a rapid recovery of amyloid-associated neuritic dystrophy in mouse models of Alzheimer's disease (Brendza *et al.*, 2005), and also previous autopsy reports of AN1792-treated patients have described a decrease in the density of clusters of dystrophic neurites upon amyloid removal (Nicoll *et al.*, 2003; Ferrer *et al.*, 2004; Masliah *et al.*, 2005). We sought to compare the amount and characteristics of plaque-associated neuritic dystrophy in hippocampal sections from the three groups of subjects. First, we counted the number of SMI312-positive dystrophic neurites and axonal swellings or spheroids within the boundaries of dense-core plaques and observed an unexpected increase in dystrophic neurites associated with the remaining plaques of AN1792-treated patients, as compared to non-immunized patients. Next, we wondered whether this resistance of dystrophic neurites to anti-Aβ immunotherapy might be due to their end-stage properties. Electron microscopy studies have described the accumulation of degenerating mitochondria in the dystrophic processes of dense-core amyloid plaques (Kidd, 1964; Fiala *et al.*, 2007). Indeed, a staging of mitochondrial degeneration has been proposed, starting with the accumulation of smaller but otherwise normal-looking mitochondria, followed by the swelling of mitochondrial cristae and the formation of lamellar bodies, and lastly clustering into multivesicular, presumably autophagic, bodies (Fiala *et al.*, 2007). We sought to depict this pathological feature with immunostaining for VDAC1 (porin, voltage-dependent anion channel type 1), a channel protein present in the outer mitochondrial membrane. As expected by these previous ultrastructural descriptions, VDAC1 decorated dystrophic processes of some dense-core plaques, intermingled with the fibrillar amyloid. Surprisingly, we found a significantly increased proportion of VDAC1-immunoreactive dense-core plaques in the immunized group. Thus, the results of this characterization of plaque-associated

neuritic dystrophy suggest that anti-Aβ active immunization might be ineffective in ameliorating amyloid-embedded end-stage dystrophic neurites unless compact amyloid is completely removed. By contrast, we postulate that the restoration of the trajectory of surrounding neurites would occur as soon as the process of plaque removal begins. Alternatively, new dystrophic neurites and axonal swellings and further mitochondrial degeneration might occur within the remaining dense-core plaques as a result of the ongoing solubilization of amyloid fibrils, perhaps due to an increase in the local concentration of toxic Aβ oligomers (Cruz *et al.*, 1997; Carulla *et al.*, 2005; Patton *et al.*, 2006; Martins *et al.*, 2008).

Previous autopsy studies of AN1792-treated patients have reported a lower density of reactive astrocyte clusters upon amyloid clearance but have not assessed the amount of astrocytosis surrounding the remaining plaques (Nicoll *et al.*, 2003; Masliah *et al.*, 2005). We measured the number of reactive astrocytes per dense core-plaque up to 50 μm from the edge of the plaques in the three study groups, and found no significant difference between plaques remaining after immunization and those from non-immunized patients, further suggesting that the former still retain toxic properties.

Notably, despite being similar in size, dense-core plaques were substantially less toxic in non-demented controls than in non-treated Alzheimer's disease patients, as judged by these measures of neuritic dystrophy and astrocytosis.

Active immunization also ameliorates the hippocampal tau pathology

In the triple transgenic mouse (3× Tg), which sequentially develops both amyloid plaques and neuronal tau aggregates, anti-Aβ immunization not only removed amyloid but also improved early tau pathology in the same sequential fashion. Yet success was not complete because late hyperphosphorylated tau aggregates remained intact after treatment (Oddo *et al.*, 2004). However, the same authors have shown that, when initiated at an earlier stage, before the mice develop plaques and tau aggregates, anti-Aβ immunization is able to prevent the development of both amyloid and tau pathologies in this mouse model (Oddo *et al.*, 2008). Recently, anti-Aβ active immunization has been shown to decrease tau hyperphosphorylation in two other mouse models that sequentially develop amyloid plaques and neuronal aggregates of hyperphosphorylated native murine tau, thus adding further evidence for its potential beneficial effect on tau pathology (Wilcock *et al.*, 2009). By contrast, previous autopsy studies of AN1792-treated patients have reported a density of neurofibrillary tangles and neuropil threads similar to non-treated patients with Alzheimer's disease and a pattern of neurofibrillary tangles distribution consistent with Braak V–VI stages. However, in a subset of 11 antibody responders with baseline and follow-up CSF samples tau levels were significantly reduced, as compared with 10 placebo recipients (Gilman *et al.*, 2005).

To analyse tau neuronal pathology, we used two different well-characterized antibodies, PHF1 and Alz50. While PHF1 binds tau protein phosphorylated at serine residues 396 and 404 (Otvos Jr. *et al.*, 1994), Alz50 is a phosphorylation-independent but conformation-dependent anti-tau antibody, with an epitope consisting of the N-terminus and one of the microtubule-binding domains of the tau molecule (Carmel *et al.*, 1996). Although both antibodies are highly specific for tau species in the Alzheimer's disease brain, Alz50 has been shown to label early misfolded tau (Carmel *et al.*, 1996), whereas PHF1 binds to later-stage hyperphosphorylated tau (Augustinack *et al.*, 2002).

Surprisingly, stereological quantification of the density of PHF1-positive neurons yielded a significant reduction in immunized patients, as compared to non-immunized patients. However, no difference was found in the quantification of Alz50 positive cells between both Alzheimer's disease groups. Furthermore, there was no significant difference between the groups in the density of late-stage thioflavin-S positive neurofibrillary tangles.

Taken together, these results suggest that anti-Aβ active immunization is able to decrease tau hyperphosphorylation but is less effective in ameliorating the misfolding and aggregation of the tau molecules. Further, they are in line with a previous autopsy study of one of these immunized patients describing a reduced immunoreactivity of phospho-tau and the stress kinases stress-activated protein kinase/c-Jun N-terminal kinase and p38 within the dystrophic neurites surrounding collapsed plaques (Ferrer *et al.*, 2004). Remarkably, among the immunized patients, both the subject who developed an autoimmune meningoencephalitis and the subject who did not generate an enzyme-linked immunosorbent assay-detectable anti-AN1792 antibody response had the highest densities of Alz50, PHF1 and thioflavin-S positive neurons. Therefore, it is possible that immunization at an earlier stage of the disease (i.e. in patients with mild cognitive impairment) would have reverted or even prevented the development of neurofibrillary tangles to a greater extent. These findings suggest a link between Aβ and tau, and provide strong support for the amyloid cascade hypothesis, which postulates that Aβ accumulation triggers the onset of Alzheimer's disease and that tau hyperphosphorylation, subsequent neurofibrillary tangles formation and neuronal death are downstream consequences of the Aβ aggregation (Hardy and Selkoe, 2002). To our knowledge, this is the first evidence of improvement of neuronal tangle pathology upon anti-Aβ immunization in patients with Alzheimer's disease. Differences with previous reports might be due to the different tau epitopes depicted in the immunohistochemical studies and to the different quantification approaches (sterology-based versus non-stereology based).

In summary, we show that clearance of amyloid plaques by anti-Aβ active immunization within the hippocampus promotes potentially beneficial structural changes of neurites and decreases the hyperphosphorylation of tau. However, dense-core plaques that remain after immunization retain at least some of their toxic properties. The morphological improvements are relatively subtle and may not be sufficient to alter the clinical course of these patients. Nonetheless, they extend previous evidence that an Aβ-directed therapy can modify the neuropathology of the human disease beyond the effects on amyloid plaques and support the idea that Aβ toxicity directly mediates at least some of the neurodegenerative phenomena associated with neural system

collapse in Alzheimer's disease. Immunization of patients at an earlier stage of the disease might enhance these positive changes and render a more robust improvement of cognitive functions. Larger clinicopathological studies on patients enrolled in ongoing active and passive immunization clinical trials are needed to confirm these results. Also, whether plaque removal by immunization leads to an increase of synaptic density or prevents further synaptic loss—the main pathological correlate of cognitive function in Alzheimer's disease—remains to be investigated.

Acknowledgements

The authors want to thank the patients and caregivers involved in research in their respective institutions.

Funding

National Institutes of Health [grant numbers AG08487 and P50AG05134 to B.T.H., M.P.F, J.H.G and C.M.W]; the Programme Hospitalier de Reserche Clinique Régional [02-029-08 to E.U.C. and M.B.D.] and the Fondo de Investigaciones Sanitarias-Instituto de Salud Carlos III of the Spanish Ministerio de Ciencia e Innovación [CM06/00161 to A.S.P.].

Supplementary material

Supplementary material is available at *Brain* online.

References

Akiyama H, Tago H, Itagaki S, McGeer PL. Occurrence of diffuse amyloid deposits in the presubicular parvopyramidal layer in Alzheimer's disease. Acta Neuropathol 1990; 79: 537–44.

Augustinack JC, Schneider A, Mandelkow EM, Hyman BT. Specific tau phosphorylation sites correlate with severity of neuronal cytopathology in Alzheimer's disease. Acta Neuropathol 2002; 103: 26–35.

Bacskai BJ, Kajdasz ST, Christie RH, Carter C, Games D, Seubert P, et al. Imaging of amyloid-β deposits in brains of living mice permits direct observation of clearance of plaques with immunotherapy. Nat Med 2001; 7: 369–72.

Bacskai BJ, Kajdasz ST, McLellan ME, Games D, Seubert P, Schenk D, et al. Non-Fc-mediated mechanisms are involved in clearance of amyloid-β in vivo by immunotheraphy. J Neurosci 2002; 22: 7873–8.

Bard F, Cannon C, Barbour R, Burke RL, Games D, Grajeda H, et al. Peripherally administered antibodies against amyloid β-peptide enter the central nervous system and reduce pathology in a mouse model of Alzheimer disease. Nat Med 2000; 6: 916–9.

Boche D, Zotova E, Weller RO, Love S, Neal JW, Pickering RM, et al. Consequence of Aβ immunization on the vasculature of human Alzheimer's disease brain. Brain 2008; 131: 3299–310.

Bombois S, Maurage CA, Gompel M, Deramecourt V, Mackowiak-Cordoliani MA, Black RS, et al. Absence of β-amyloid deposits after immunization in Alzheimer disease with Lewy body dementia. Arch Neurol 2007; 64: 583–7.

Braak H, Braak E. Neuropathological stageing of Alzheimer-related changes. Acta Neuropathol 1991; 82: 239–59.

Brendza RP, Bacskai BJ, Cirrito JR, Simmons KA, Skoch JM, Klunk WE, et al. Anti-Aβ antibody treatment promotes the rapid recovery of amyloid-associated neuritic dystrophy in PDAPP transgenic mice. J Clin Invest 2005; 115: 428–33.

Buttini M, Masliah E, Barbour R, Grajeda H, Motter R, Johnson-Wood K, et al. β-amyloid immunotherapy prevents synaptic degeneration in a mouse model of Alzheimer's disease. J Neurosci 2005; 25: 9096–101.

Carmel G, Mager EM, Binder LI, Kuret J. The structural basis of monoclonal antibody Alz50's selectivity for Alzheimer's disease pathology. J Biol Chem 1996; 51: 32789–95.

Carulla N, Caddy GL, Hall DR, Zurdo J, Gairi M, Feliz M, et al. Molecular recycling within amyloid fibrils. Nature 2005; 436: 554–8.

Cruz L, Urbanc B, Buldyrev SV, Christie R, Gómez-Isla T, Havlin S, et al. Aggregation and disaggregation of senile plaques in Alzheimer disease. Proc Natl Acad Sci 1997; 94: 7612–6.

D'Amore JD, Kajdasz ST, McLellan ME, Bacskai BJ, Stern EA, Hyman BT. In vivo multiphoton imaging of a transgenic mouse model of Alzheimer disease reveals marked thioflavin-S-associated alterations in neurite trajectories. J Neuropathol Exp Neurol 2003; 62: 137–45.

DeKosky ST, Scheff SW. Synapse loss in frontal cortex biopsies in Alzheimer's disease: Correlation with cognitive severity. Ann Neurol 1990; 27: 457–64.

DeMattos RB, Bales KR, Cummins DJ, Dodart JC, Paul SM, Holtzman DM. Peripheral anti-Aβ antibody alters CNS and plasma Aβ clearance and decreases brain Aβ burden in a mouse model of Alzheimer's disease. Proc Natl Acad Sci 2001; 98: 8850–5.

Dodart JC, Bales KR, Gannon KS, Greene SJ, DeMattos RB, Mathis C, et al. Immunization reverses memory deficits without reducing brain Aβ burden in Alzheimer's disease model. Nat Neurosci 2002; 5: 452–7.

Ferrer I, Boada-Rovira M, Sánchez-Guerra ML, Rey MJ, Costa-Jussá F. Neuropathology and pathogenesis of encephalitis following amyloid-β immunization in Alzheimer's disease. Brain Pathol 2004; 14: 11–20.

Fiala JC, Feinberg M, Peters A, Barbas H. Mitochondrial degeneration in dystrophic neurites of senile plaques may lead to extracellular deposition of fine filaments. Brain Struct Funct 2007; 212: 195–207.

Gilman S, Koller M, Black RS, Jenkins L, Griffith SG, Fox NC, et al. Clinical effects of Aβ immunization (AN1792) in patients with AD in an interrupted trial. Neurology 2005; 64: 1553–62.

Gómez-Isla T, Price JL, McKeel DW Jr, Morris JC, Growdon JH, Hyman BT. Profound loss of layer II entorhinal cortex neurons occurs in very mild Alzheimer's disease. J Neurosci 1996; 16: 4491–500.

Gómez-Isla T, Hollister R, West H, Mui S, Growdon JH, Petersen RC, et al. Neuronal loss correlates with but exceeds neurofibrillary tangles in Alzheimer's disease. Ann Neurol 1997; 41: 17–24.

Hardy J, Selkoe DJ. The amyloid hypothesis of Alzheimer's disease: progress and problems on the road to therapeutics. Science 2002; 297: 353–6.

Hock C, Konietzko U, Streffer JR, Tracy J, Signorell A, Müller-Tillmanns B, et al. Antibodies against β-amyloid slow cognitive decline in Alzheimer's disease. Neuron 2003; 38: 547–54.

Holmes C, Boche D, Wilkinson D, Yadegarfar G, Hopkins V, Bayer A, et al. Long-term effects of $A\beta_{42}$ immunisation in Alzheimer's disease: follow-up of a randomised, placebo-controlled phase I trial. Lancet 2008; 372: 216–23.

Hyman BT, Gómez-Isla T, Irizarry MC. Stereology: a practical primer for neuropathology. J Neuropathol Exp Neurol 1998; 57: 305–10.

Janus C, Pearson J, McLaurin J, Mathews PM, Jiang Y, Schmidt SD, et al. Aβ immunization reduces behavioural mathewsimpairment and plaques in a model of Alzheimer's disease. Nature 2000; 408: 979–82.

Kalus P, Braak H, Braak E, Bohl J. The presubicular region in Alzheimer's disease: topography of amyloid deposits and neurofibrillary changes. Brain Res 1989; 494: 198–203.

Kidd M. Alzheimer's disease. An electron microscopical study. Brain 1964; 87: 307–20.

Knowles RB, Wyart C, Buldyrev SV, Cruz L, Urbanc B, Hasselmo ME, et al. Plaque-induced neurite abnormalities: implications for disruption

of neural networks in Alzheimer's disease. Proc Natl Acad Sci 1999; 96: 5274–9.

Kotilinek LA, Bacskai B, Westerman M, Kawarabayashi T, Younkin L, Hyman BT, et al. Reversible memory loss in a mouse transgenic model of Alzheimer's disease. J Neurosci 2002; 22: 6331–5.

Lee M, Bard F, Johnson-Wood K, Lee C, Hu K, Griffith SG, et al. Aβ42 immunization in Alzheimer's disease generates Aβ N-terminal antibodies. Ann Neurol 2005; 58: 430–5.

Lemere CA, Spooner ET, LaFrancois J, Malester B, Mori C, Leverone JF, et al. Evidence for peripheral clearance of cerebral Aβ protein following chronic, active Aβ immunization in PSAPP mice. Neurobiol Dis 2003; 14: 10–8.

Lombardo JA, Stern ES, McLellan ME, Kajdasz ST, Hickey GA, Bacskai BJ, et al. Amyloid-β antibody treatment leads to rapid normalization of plaque-induced neuritic alterations. J Neurosci 2003; 23: 10879–83.

Martins IC, Kupperstein I, Wilkinson H, Maes E, Vanbrabant M, Jonckheere W, et al. Lipids revert inert Aβ amyloid fibrils to neurotoxic protofibrils that affect learning in mice. Embo J 2008; 27: 224–33.

Masliah E, Hansen L, Adame A, Crews L, Bard F, Lee C, et al. Aβ vaccination effects on plaque pathology in the absence of encephalitis in Alzheimer disease. Neurology 2005; 64: 129–31.

Meyer-Luehmann M, Spires-Jones TL, Prada C, García-Alloza M, de Calignon A, Rozkalne A, et al. Rapid appearance and local toxicity of amyloid-β plaques in a mouse model of Alzheimer's disease. Nature 2008; 451: 720–5.

Morgan D, Diamond DM, Gottschall PE, Ugen KE, Dickey C, Hardy J, et al. Aβ peptide vaccination prevents memory loss in an animal model of Alzheimer's disease. Nature 2000; 408: 982–5.

Nicoll JAR, Wilkinson D, Holmes C, Steart P, Markham H, Weller RO. Neuropathology of human Alzheimer disease after immunization with amyloid-β peptide: a case report. Nat Med 2003; 9: 448–52.

Oddo S, Billings L, Kesslak JP, Cribbs DH, LaFerla FM. Aβ immunotherapy leads to clearance of early, but not late, hyperphosphorylated tau aggregates via the proteasome. Neuron 2004; 43: 321–32.

Oddo S, Caccamo A, Tseng B, Cheng D, Vasilevko V, Cribbs DH, et al. Blocking $A\beta_{42}$ accumulation delays the onset and progression of tau pathology via the C terminus of Heat Shock Protein70-Interacting Protein: a mechanistic link between Aβ and tau pathology. J Neurosci 2008; 28: 12163–75.

Orgogozo JM, Gilman S, Dartigues JF, Laurent B, Puel M, Kirby LC, et al. Subacute meningoencephalitis in a subset of patients with AD after Aβ42 immunization. Neurology 2003; 61: 46–54.

Otvos L Jr, Feiner L, Lang E, Szendrei GI, Goedert M, Lee VMY. Monoclonal antibody PHF-1 recognizes tau protein phosphorylated at serine residues 396 and 404. J Neurosci Res 1994; 39: 669–73.

Patton RL, Kalback WM, Esh CL, Kokjohn TA, Van Vickle GD, Luehrs DC, et al. Amyloid-β peptide remnants in AN-1792-immunized Alzheimer's disease patients. A biochemical analysis. Am J Pathol 2006; 169: 1048–63.

Schenk D, Barbour R, Whitney D, Gordon G, Grajeda H, Guido T, et al. Immunization with amyloid-β attenuates Alzheimer-disease-like pathology in the PDAPP mouse. Nature 1999; 400: 173–7.

Spires-Jones TL, Mielke ML, Rozkalne A, Meyer-Luehmann M, de Calignon A, Bacskai BJ, et al. Passive immunotheraphy rapidly increases structural plasticity in a mouse model of Alzheimer disease. Neurobiol Dis 2009; 33: 213–20.

Stern EA, Bacskai BJ, Hickey GA, Attenello FJ, Lombardo JA, Hyman BT. Cortical synaptic integration in vivo is disrupted by amyloid-β plaques. J Neurosci 2004; 24: 4535–40.

Terry RD, Masliah E, Salmon DP, Butters N, DeTeresa R, Hill R, et al. Physical basis of cognitive alterations in Alzheimer's disease: synapse loss is the major correlate of cognitive impairment. Ann Neurol 1991; 30: 572–80.

Uro-Coste E, Russano de Paiva G, Guilbeau-Frugier C, Sastre N, Ousset PJ, Adolfo da Silva N, et al. Cerebral amyloid angiopathy and microhaemorrhages after amyloid β vaccination: case report and brief review. Clin Neuropathol 2010 in press.

Vellas B, Black R, Thal LJ, Fox NC, Daniels M, McLennan G, et al. Long-term follow-up of patients immunized with AN1792: reduced functional decline in antibody responders. Curr Alzheimer Res 2009; 6: 144–51.

Wilcock DM, Rojiani A, Rosenthal A, Levkowitz G, Subbarao S, Alamed J, et al. Passive amyloid immunotherapy clears amyloid and transiently activates microglia in a transgenic mouse model of amyloid deposition. J Neurosci 2004; 24: 6144–51.

Wilcock DM, Gharkholonarche N, Van Nostrand WE, Davis J, Vitek MP, Colton CA. Amyloid reduction by amyloid-β vaccination also reduces mouse tau pathology and protects from neuron loss in two mouse models of Alzheimer's disease. J Neurosci 2009; 29: 7957–65.

Wisniewski HM, Sadowski M, Jakubowska-Sadowska K, Tarnawski M, Wegiel J. Diffuse, lake-like amyloid-β deposits in the parvopyramidal layer of the presubiculum in Alzheimer disease. J Neuropathol Exp Neurol 1998; 57: 674–83.